RSC Advances

PAPER

View Article Online
View Journal | View Issue

Cite this: *RSC Adv.*, 2017, **7**, 2555

Sonochemical one pot synthesis of novel spiroacridines catalyzed by magnetically functionalized Fe_3O_4 nanoparticles with chitosan as a reusable effective catalyst†

Hossein Naeimi* and Sepideh Lahouti

A facile one-pot and three-component economical synthesis of spiroacridine using acenaphthoquinone, different anilines and dimedone in the presence of Fe_3O_4@CS–SO_3H NPs catalyst under ultrasonic irradiation is described. Firstly, the Fe_3O_4@CS NPs were prepared from reaction of chitosan with Fe_3O_4 NPs. Afterwards, treatment of Fe_3O_4@CS NPs with chlorosulfonic acid leads to the formation of Fe_3O_4@CS–SO_3H NPs. Compared to the conventional methods, the ultrasound procedure showed several advantages including mild reaction conditions, high yield of products, short reaction times, and reusability of the catalyst. The core–shell structure and the composition of the produced magnetic nanocatalyst were analyzed using FT-IR, XRD, VSM, SEM and EDX techniques.

Received 6th November 2016
Accepted 29th November 2016

DOI: 10.1039/c6ra26386k

www.rsc.org/advances

1. Introduction

Ultrasound irradiation has been considered to be a clean and beneficial protocol in organic synthesis in the last three decades.[1] The role of sonochemistry in the development of "benign by-design" synthetic procedures is clear from the description: low level of wastage, inherent safety, material and energy saving, with an optimized use of nonrenewable resources, and a preferential operation of renewable ones.[2] The application of ultrasound in organic synthesis has been increasing because of its advantages such as shorter reaction times, milder reaction condition, and higher yields in analogy with the classical methods.[3–5] Spiro compounds having cyclic structures fused at a central carbon are of recent interest because of their interesting conformational features and their structural implications on biological systems.[6–8]

The synthesis of spiro-heterocycles presents an interesting synthetic challenge to organic chemists because of its structural rigidity and complexity. Nitrogen inclosing spiro-heterocycles display remarkable biological properties, and are also frequently observed in natural products such as paraherquamide A, spirotryprostatin A, spirotryprostatin B, mitraphylline, pteropodine, and isopteropodine (Fig. 1).[9]

Generally, many synthetic analogs containing an oxindole also display antiparasitic, antibacterial, antimicrobial, antimycobacterial, antitubercular, anticancer, analgesic and anti-inflammatory, and anti-HIV activities.[10–13] Spirocyclic systems including one carbon atom common to two rings are structurally interesting.[14] The attendance of the sterically forced spiro structure in various natural products also adds to the interest in the investigations of spiro compounds.[15] Spiro compounds represent an important class of naturally happening substances characteristic by their highly pronounced biological properties. Similarly, functionalized spiro cycloalkyloxindoles are found in a diversity of natural products and bioactive molecules.[16] Nanomaterials collected together result in multifunctional nanostructures having innovative industrial and biomedical applications.[17]

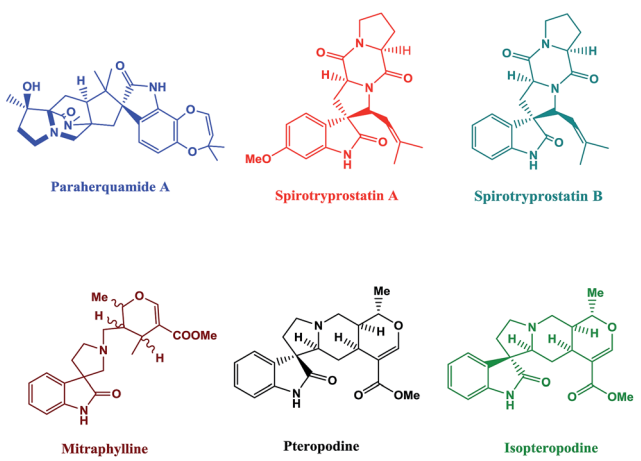

Fig. 1 Natural products possessing spiro-centres.

Department of Organic Chemistry, Faculty of Chemistry, University of Kashan, Kashan, 87317, I.R. Iran. E-mail: naeimi@kashanu.ac.ir; Fax: +98 3155912397; Tel: +98 3155912388

† Electronic supplementary information (ESI) available. See DOI: 10.1039/c6ra26386k

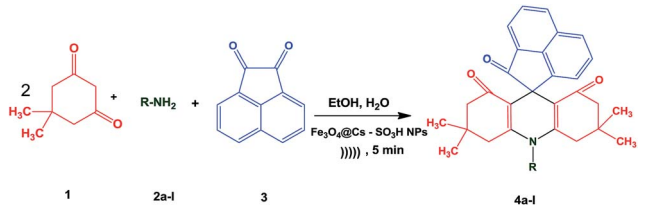

Scheme 1 Various synthesized spiroacridine in the presence of Fe_3O_4@CS–SO_3H NPs.

In recent decades, scrambles have been prepared combine different types of nanoparticles (NPs) in order to attain superior composite material properties.[18] The magnetic iron(III) oxides NPs (Fe_3O_4 and γ-Fe_2O_3) have absorbed consideration because of their magnetic property.[19–21] Functionalization and modification of the surface of the Fe_3O_4 nanoparticles with different biocompatible and biodegradable polymers have been widely tested because the introduction of new substance could also bring new functions for magnetite.[22–25] Chitosan is a partially acetylated glucosamine biopolymer with many useful features such as hydrophilicity, biocompatibility, and biodegradability.[26] Chitosan, due to its high amino content, has been found to possess good absorption capacity for many heavy metal ions through complexation with the amine groups. It has been widely used as biosorbent for removing different metal ions from wastewater. Furthermore, due to magnetic properties, it can easily be separated from the sorption system by using magnetic field.[27–29]

We report herein a clean synthesis of spiroacridine derivatives from a wide of acenaphthoquinone, different anilines and dimedone compounds in the presence of Fe_3O_4@CS–SO_3H NPs under ultrasonic irradiation. The high yields, and the possibility of easy recovering of the catalyst are the most advantages of this method (Scheme 1).

2. Experimental section

2.1. Materials

The chemicals used in this work were obtained from Fluka and Merck Chemical Company and were used without purification.

2.2. Apparatus

FT-IR spectra were obtained with potassium bromide pellets in the range 400–4000 cm^{-1} with a Perkin-Elmer 550 spectrometer. ^1H NMR and ^{13}C NMR spectra were recorded with a Bruker DRX-400 spectrometer at 400 and 100 MHz respectively. NMR spectra were reported as parts per million (ppm) downfield from tetramethylsilane as internal standard. The abbreviations used are: singlet (s), doublet (d), triplet (t) and multiplet (m). Nanostructures were characterized using a Holland Philips Xpert X-ray powder diffraction (XRD) diffractometer (CuK, radiation, k = 0.154056 nm), at a scanning speed of 2° min^{-1} from 10° to 100° (2θ). A BANDELIN ultrasonic HD 3200 with probe model KE 76, with the diameter of 6 mm, was used to produce ultrasonic irradiation and homogenizing the reaction mixture. Piezoelectric crystal of this kind of probe normally works in the range of 700 kHz, but by using some proper clamps, the output frequency of piezoelectric crystal have controlled and reduced to 20 kHz. Therefore, the induced frequency of probe to the reaction mixture is equal to 20 kHz. A thermal method was used for the calibration of ultrasonic power. Melting points are determined in open capillaries using an Electrothermal Mk3 apparatus and are uncorrected. The purity determination of the substrates and reaction monitoring were accomplished by TLC on silica-gel polygram SILG/UV 254 plates (from Merck Company). FE-SEM images of the products were visualized by a Sigma ZEISS, Oxford Instruments Field Emission Scanning Electron Microscope. The magnetic properties of nanoparticles have been measured with a vibrating sample magnetometer (VSM, PPMS-9T) at 300 K in Iran (University of Kashan).

2.3. General information

2.3.1 Typical experimental procedure for the preparation of chitosan-coated magnetic nanoparticles Fe_3O_4@CS NPs. Fe_3O_4@CS NPs were prepared using chemical co-precipitation described in the literature. In short, 1.5 g of chitosan (molecular weight: 100 000–300 000) is dissolved in 25 mL of 0.05 M acetic acid solution; to which $FeCl_2 \cdot 4H_2O$ (1.29 g, 0.5 mmol) and $FeCl_3 \cdot 6H_2O$ (3.51 g, 0.25 mmol) are added. The resulting solution is mechanically stirred for 6 h at 80 °C, under N_2 atmosphere. Consequently, 6 mL of 25% NH_4OH is injected drop wise into the reaction mixture with constant stirring. After 40 min, the mixture is cooled to room temperature and chitosan coated over magnetic nanoparticles were separated by magnetic decantation and washed three times with distilled water, then ethanol, and finally dried under vacuum at room temperature.

2.4. Preparation of sulfonated chitosan encapsulated nano iron oxide Fe_3O_4@CS–SO_3H NPs

Fe_3O_4@CS NPs (10 mg) is dispersed in dry CH_2Cl_2 (2 mL) and sonicated for 20 min, then chlorosulfonic acid (0.3 mL) is added drop-wise over a period of 10 min, at room temperature under N_2 atmosphere. Subsequently, the mixture is mechanically stirred for 15 min until HCl gas evolution is stopped. Finally, functionalized magnetic Fe_3O_4@CS–SO_3H NPs is separated by an external magnet, washed several times with dry CH_2Cl_2, until a neutral pH level is achieved, then dried under vacuum at room temperature (Scheme 2).

In order to determine the acid strength of catalyst, a 0.08 M solution of sodium hydroxide was used for measurement of total surface acidity for the Fe_3O_4@CS–SO_3H NPs. Then, 0.02 g of solid was suspended in this solution for 18 h, and the excess amount of base was titrated against the hydrochloric acid using phenolphthalein as an indicator.

2.5. General procedure for the synthesis of spiroacridines catalyzed by Fe_3O_4@CS–SO_3H NPs

2.5.1 Typical heating method. In a typical spiroacridine synthesis, 1,3-indandione (2 mmol), aniline (1 mmol), acenaphthoquinone (1 mmol), and Fe_3O_4@CS–SO_3H NPs (15 mol%) in refluxing aqueous ethanol (5 : 1, v/v) (5 mL) was

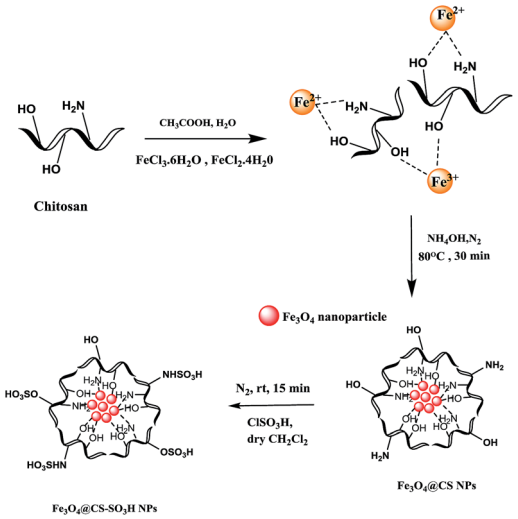

Scheme 2 Preparation steps of Fe_3O_4@CS–SO_3H NPs.

stirred for 60 min. After the reaction was completed, the catalyst was separated by an external magnet. The reaction mixture was cooled to room temperature. Then, the precipitated product was filtered and washed ethanol to afford the pure product.

2.5.2 Ultrasound irradiation. The dimedone (1) (2 mmol), aniline (2) (1 mmol), acenaphthoquinone (3) (1 mmol), Fe_3O_4@CS–SO_3H NPs (15 mol%) and aqueous ethanol (5 : 1, v/v) (5 mL) were added into a 25 mL round bottomed flask. The reaction mixture was sonicated under 40 W for the period of time (the reaction was monitored by TLC). The reaction mixture was filtered and the precipitate washed with ethanol. The crude solid product was recrystallized from ethanol to give pure spiroacridine as a target product. Then, all of the products were identified by IR, ^{1}H NMR, ^{13}C NMR and C.H.N analyses.

2.6. Representative spectral data

2.6.1 (4-Nitrophenyl)spiro[acenaphthylene-1,9′-acridine]trione (4a). Orange solid, mp > 300 °C. IR (KBr) ν: 3610, 3475, 3358, 2961, 1717, 1612 cm^{-1}; ^{1}H NMR (400 MHz, DMSO-d_6) δ: 8.09 (d, 2H, ArH), 7.20–7.94 (m, 7H, ArH), 6.84 (s, 1H, ArH), 1.56–2.31 (m, 8H, 4CH_2), 0.88–1.25 (m, 12H, 4CH_3) ppm; ^{13}C NMR (100 MHz, DMSO-d_6) δ: 26.4, 30.5, 41.1, 46.2, 55.8, 106.9, 114.2, 116.7, 121.2, 123.6, 125.3, 126.5, 127.1, 130.6, 131.7, 132.6, 133.5, 135.2, 141.1, 152.5, 156.4, 159.6, 192.3, 202.5, 204.7 ppm. Anal. calcd for $C_{34}H_{30}N_2O_5$: C, 74.71; H, 5.53; N, 5.12. Found: C, 74.59; H, 5.61; N, 4.98.

2.6.2 (4-Hydroxyphenyl)spiro[acenaphthylene-1,9′-acridine]-trione (4b). Orange solid, mp > 300 °C. IR (KBr) ν: 3613, 3460, 3347, 2932, 1710, 1617 cm^{-1}; ^{1}H NMR (400 MHz, DMSO-d_6) δ: 8.73 (d, 2H, ArH), 8.26 (t, 3H, ArH), 7.93 (d, 2H, ArH), 7.89 (s, 1H, OH), 7.12 (d, 2H, ArH), 6.82–7.33 (d, 2H, ArH), 1.75–2.32 (m, 8H, 4CH_2), 0.95–1.14 (m, 12H, 4CH_3) ppm; ^{13}C NMR (100 MHz, DMSO-d_6) δ: 27.8, 32.5, 41.1, 45.2, 54.8, 105.9, 112.2, 115.7, 120.2, 122.6, 124.3, 126.7, 127.2, 130.8, 131.5, 132.7, 134.5, 136.2, 142.1, 154.5, 158.4, 159.1, 193.3, 203.5, 204.4 ppm. Anal. calcd for $C_{34}H_{31}NO_4$: C, 78.89; H, 6.04; N, 2.71. Found: C, 78.81; H, 5.93; N, 2.59.

2.6.3 (4-Chlorophenyl)spiro[acenaphthylene-1,9′-acridine]trione (4c). Orange solid, mp > 300 °C. IR (KBr) ν: 3358, 2961, 2870, 1723, 1609 cm^{-1}; ^{1}H NMR (400 MHz, DMSO-d_6) δ: 6.95–8.86 (m, 10H, ArH), 1.60–2.22 (m, 8H, 4CH_2), 0.75–1.14 (m, 12H, 4CH_3) ppm; ^{13}C NMR (100 MHz, DMSO-d_6) δ: 27.9, 32.5, 42.1, 48.2, 57.8, 108.9, 112.2, 115.7, 121.2, 122.6, 124.3, 126.5, 129.1, 130.6, 131.8, 132.6, 134.5, 135.2, 140.1, 154.5, 158.4, 158.6, 189.3, 201.5, 203.7 ppm. Anal. calcd for $C_{34}H_{30}NO_3Cl$: C, 76.18; H, 5.64; N, 2.61. Found: C, 76.05; H, 5.72; N, 2.75.

2.6.4 (4-Bromophenyl)spiro[acenaphthylene-1,9′-acridine]trione (4d). Orange solid, mp > 300 °C. IR (KBr) ν: 3362, 2942, 2854, 1712, 1626 cm^{-1}; ^{1}H NMR (400 MHz, DMSO-d_6) δ: 8.26 (d, J = 7.2, 2H, ArH), 7.81 (d, J = 7.2, 5H, ArH), 7.56 (d, J = 7.2, 2H, ArH), 7.21 (s, 1H, ArH), 1.70–2.36 (m, 8H, 4CH_2), 0.96–1.10 (m, 12H, 4CH_3) ppm; ^{13}C NMR (100 MHz, DMSO-d_6) δ: 27.1, 33.5, 40.1, 47.2, 55.8, 107.9, 111.2, 114.7, 120.2, 123.6, 125.3, 127.5, 128.1, 129.6, 132.8, 133.6, 134.7, 136.2, 140.7, 157.5, 158.4, 159.6, 190.3, 202.5, 205.7 ppm. Anal. calcd for $C_{34}H_{30}NO_3Br$: C, 70.35; H, 5.21; N, 2.41. Found: C, 70.22; H, 5.10; N, 2.30.

2.6.5 (*p*-Tolyl)spiro[acenaphthylene-1,9′-acridine]trione (4e). Orange solid, mp > 300 °C. IR (KBr) ν: 3451, 3143, 2940, 1662, 1606 cm^{-1}; ^{1}H NMR (400 MHz, DMSO-d_6) δ: 8.33 (s, 1H, ArH), 8.25 (d, J = 7.2 Hz, 2H, ArH), 7.92 (t, J = 7.2 Hz, 2H, ArH), 7.43–7.73 (m, J = 7.2 Hz, 3H, ArH), 7.28 (d, J = 7.8 Hz, 2H, ArH), 7.10 (d, J = 7.8 Hz, 1H, ArH), 2.51–2.84 (m, 8H, 4CH_2), 2.43 (s, 3H, CH_3), 0.85–1.12 (m, 12H, 4CH_3) ppm; ^{13}C NMR (100 MHz, DMSO-d_6) δ: 28.2, 32.1, 47.1, 51.4, 54.8, 57.3, 108.7, 112.1, 119.3, 121.8, 124.0, 125.5, 127.9, 128.9, 130.6, 131.1, 133.6, 135.8, 138.7, 141.0, 157.6, 158.1, 165.6, 192.3, 205.5, 207.7 ppm. Anal. calcd for $C_{35}H_{33}NO_3$: C, 81.52; H, 6.45; N, 2.72. Found: C, 81.38; H, 6.34; N, 2.61.

2.6.6 (4-Methoxyphenyl)spiro[acenaphthylene-1,9′-acridine]-trione (4f). Orange solid, mp > 300 °C. IR (KBr) ν: 3371, 3043, 2908, 1688, 1603 cm^{-1}; ^{1}H NMR (400 MHz, DMSO-d_6) δ: 8.55 (s, 1H, ArH), 8.15 (d, J = 7.2 Hz, 2H, ArH), 7.90 (t, J = 7.2 Hz, 2H, ArH), 7.52–7.79 (m, J = 7.2 Hz, 5H, ArH), 7.09 (d, J = 7.8 Hz, 2H, ArH), 6.93 (d, J = 7.8 Hz, 2H, ArH), 3.89 (s, 3H, OCH_3), 1.79–2.34 (m, 8H, 4CH_2), 0.88–1.12 (m, 12H, 4CH_3) ppm; ^{13}C NMR (100 MHz, DMSO-d_6) δ: 27.2, 33.1, 44.1, 51.2, 55.8, 56.3, 109.7, 113.1, 117.3, 121.1, 122.0, 125.2, 128.9, 129.9, 130.6, 131.8, 132.6, 135.7, 136.7, 142.0, 156.6, 158.6, 159.6, 190.3, 204.5, 206.7 ppm. Anal. calcd for $C_{35}H_{33}NO_4$: C, 79.07; H, 6.26; N, 2.63. Found: C, 78.94; H, 6.19; N, 2.69.

2.6.7 (2-Hydroxyphenyl)spiro[acenaphthylene-1,9′-acridine]-trione (4g). Orange solid, mp > 300 °C. IR (KBr) ν: 3513, 3454, 3347, 2942, 1715, 1625 cm^{-1}; ^{1}H NMR (400 MHz, DMSO-d_6) δ: 7.76 (s, 1H, ArH), 7.73 (s, 1H, ArH), 7.65 (d, J = 7.2, 2H, ArH), 7.59 (d, J = 7.2, 2H, ArH), 7.44 (s, 1H, ArH), 7.42 (s, 1H, ArH), 7.41 (s, 1H, ArH), 7.39 (s, 1H, ArH), 7.37 (s, 1H, ArH), 2.45 (s, 2H, CH_2), 2.26 (s, 2H, CH_2), 2.15 (s, 2H, CH_2), 1.83 (s, 2H, CH_2), 0.98–1.10 (m, 12H, 4CH_3) ppm; ^{13}C NMR (100 MHz, DMSO-d_6) δ: 28.8, 31.5, 40.1, 44.2, 52.8, 107.9, 113.2, 114.7, 119.2, 122.6, 125.3, 126.7, 128.2, 130.8, 132.5, 132.7, 135.5, 136.7, 144.1, 156.5, 158.1, 159.4, 192.3, 202.5, 205.4 ppm. Anal. calcd for $C_{34}H_{31}NO_4$: C, 78.89; H, 6.04; N, 2.71. Found: C, 78.81; H, 5.93; N, 2.59.

2.6.8 (2-Nitrophenyl)spiro[acenaphthylene-1,9′-acridine]trione (4h). Orange solid, mp > 300 °C. IR (KBr) ν: 3604, 3460,

3351, 2942, 1719, 1609 cm^{-1}; ^1H NMR (400 MHz, DMSO-d_6) δ: 7.26–8.09 (m, 10H, ArH), 2.01–2.15 (m, 8H, $4CH_2$), 0.90–1.20 (m, 12H, $4CH_3$) ppm; ^{13}C NMR (100 MHz, DMSO-d_6) δ: 27.1, 31.5, 44.1, 45.2, 52.8, 108.9, 113.2, 118.7, 120.2, 122.6, 125.4, 126.1, 128.1, 129.6, 131.7, 132.4, 134.5, 135.7, 142.1, 153.5, 155.4, 158.6, 193.3, 203.5, 205.7 ppm. Anal. calcd for $C_{34}H_{30}N_2O_5$: C, 74.71; H, 5.53; N, 5.12. Found: C, 74.59; H, 5.61; N, 4.98.

2.6.9 (2-Chlorophenyl)spiro[acenaphthylene-1,9′-acridine] trione (4i). Orange solid, mp > 300 °C. IR (KBr) ν: 3348, 2967, 2855, 1714, 1611 cm^{-1}; ^1H NMR (400 MHz, DMSO-d_6) δ: 8.42 (d, 2H, ArH), 8.09 (s, 1H, ArH), 7.95 (d, 3H, ArH), 7.90 (d, 2H, ArH), 7.83 (d, 2H, ArH), 2.25 (s, 8H, $4CH_2$), 0.75–1.10 (m, 12H, $4CH_3$) ppm; ^{13}C NMR (100 MHz, DMSO-d_6) δ: 28.5, 31.5, 43.1, 46.2, 58.8, 110.9, 111.5, 114.7, 120.2, 123.6, 125.3, 127.5, 129.4, 130.7, 131.7, 132.1, 133.5, 135.4, 144.1, 155.2, 158.4, 159.6, 190.3, 202.5, 204.7 ppm. Anal. calcd for $C_{34}H_{30}NO_3Cl$: C, 76.18; H, 5.64; N, 2.61. Found: C, 76.05; H, 5.72; N, 2.75.

2.6.10 (3-Nitrophenyl)spiro[acenaphthylene-1,9′-acridine] trione (4j). Orange solid, mp > 300 °C. IR (KBr) ν: 3594, 3451, 3324, 2935, 1714, 1604 cm^{-1}; ^1H NMR (400 MHz, DMSO-d_6) δ: 7.82 (d, 2H, ArH), 7.55 (d, 3H, ArH), 7.37 (d, 3H, ArH), 7.24 (d, 2H, ArH), 1.85–2.30 (m, 8H, $4CH_2$), 0.96–1.15 (m, 12H, $4CH_3$) ppm; ^{13}C NMR (100 MHz, DMSO-d_6) δ: 28.1, 32.1, 44.7, 45.4, 53.8, 109.9, 112.2, 118.4, 121.2, 123.6, 125.4, 128.1, 128.7, 129.4, 131.4, 132.1, 134.6, 136.7, 143.1, 154.5, 155.4, 159.6, 195.3, 202.5, 205.2 ppm. Anal. calcd for $C_{34}H_{30}N_2O_5$: C, 74.71; H, 5.53; N, 5.12. Found: C, 74.59; H, 5.61; N, 4.98.

2.6.11 (2,4-Dimethylphenyl)spiro[acenaphthylene-1,9′-acridine]trione (4k). Orange solid, mp > 300 °C. IR (KBr) ν: 3604, 3425, 3328, 2937, 1722, 1608 cm^{-1}; ^1H NMR (400 MHz, DMSO-d_6) δ: 6.68–8.29 (m, 9H, ArH), 1.14–2.05 (m, 8H, $4CH_2$), 0.73–1.12 (m, 12H, $4CH_3$) ppm; ^{13}C NMR (100 MHz, DMSO-d_6) δ: 27.2, 33.1, 43.7, 45.4, 54.8, 108.9, 113.2, 119.4, 122.2, 124.6, 126.4, 127.1, 128.7, 129.7, 130.4, 132.1, 133.6, 135.7, 142.1, 153.5, 156.4, 158.6, 196.3, 204.5, 205.7 ppm. Anal. calcd for $C_{36}H_{36}NO_3$: C, 81.63; H, 6.66; N, 2.64. Found: C, 81.50; H, 6.51; N, 2.79.

2.6.12 (Benzyl)spiro[acenaphthylene-1,9′-acridine]trione (4l). Orange solid, mp > 300 °C. IR (KBr) ν: 3351, 3243, 2840, 1652, 1604 cm^{-1}; ^1H NMR (400 MHz, DMSO-d_6) δ: 8.34 (s, 1H, ArH), 8.27 (s, 1H, ArH), 8.07 (s, 1H, ArH), 7.80 (d, J = 7.2 Hz, 2H, ArH), 7.33 (d, J = 7.8 Hz, 2H, ArH), 7.21 (t, J = 7.8 Hz, 3H, ArH), 6.97 (s, 1H, ArH), 2.02–2.36 (m, 8H, $4CH_2$), 1.93 (s, 2H, CH_2), 0.96–1.13 (m, 12H, $4CH_3$) ppm; ^{13}C NMR (100 MHz, DMSO-d_6) δ: 27.6, 33.1, 46.1, 52.4, 55.8, 56.3, 109.7, 114.1, 120.3, 122.8, 123.0, 126.5, 127.9, 129.9, 130.6, 131.1, 132.6, 134.8, 139.7, 142.0, 156.6, 158.1, 167.6, 194.3, 204.5, 206.7 ppm. Anal. calcd for $C_{35}H_{33}NO_3$: C, 81.52; H, 6.45; N, 2.72. Found: C, 81.38; H, 6.34; N, 2.61.

2.6.13 (1,4-Phenylene)spiro[acenaphthylene-1,9′-acridine] trione (4m). Brown solid, mp > 300 °C. IR (KBr) ν: 3384, 2957, 1721, 1604, 1512, 1465 cm^{-1}; ^1H NMR (400 MHz, DMSO-d_6) δ: 8.44 (d, 1H, ArH), 8.07 (s, 2H, ArH), 7.91 (m, 3H, ArH), 7.77 (d, J = 7.2 Hz, 2H, ArH), 2.08–2.23 (m, 8H, $4CH_2$), 1.22 (d, 6H, $2CH_3$), 1.05 (s, 3H, CH_3), 0.98 (s, 3H, CH_3) ppm. Anal. calcd for $C_{62}H_{56}N_2O_6$: C, 80.49; H, 6.10; N, 3.03. Found: C, 80.38; H, 6.11; N, 3.07.

3. Results and discussion

3.1. Preparation and characterization of Fe_3O_4@CS–SO_3H NPs

Fe_3O_4@CS–SO_3H NPs was prepared according to a modified procedure in the literature (Scheme 1). The Fe_3O_4 MNPs were prepared by the well-known Massart's method[30] which consists of Fe(III) and Fe(II) co-precipitation with molar ratio 2 : 1. Then, the synthesized magnetic nanoparticles were modified with chitosan as a natural polymer. The resulting solution is mechanically stirred for 6 h at 80 °C under N_2 atmosphere. The NH_4OH is injected drop wise into the reaction mixture with constant stirring for 30 min. Fe_3O_4@CS NPs is dispersed in dry CH_2Cl_2 in an ultrasonic bath for 20 min, then chlorosulfonic acid is added. The magnetically heterogeneous organocatalyst, Fe_3O_4@CS–SO_3H NPs, is characterized by X-ray diffraction (XRD), scanning electron microscopy (SEM), energy-dispersive X-ray spectroscopy (EDX), vibrating sample magnetometer (VSM) and Fourier transform infrared (FT-IR) spectroscopy.

3.1.1 FT-IR analysis. The FT-IR spectra of (a) chitosan, (b) Fe_3O_4@CS NPs and (c) Fe_3O_4@CS–SO_3H NPs are instructive (Fig. 2). In addition, the O–H stretching vibration at 3428 and 3433 cm^{-1} were detected in peaks of Fig. 2a–c. The FT-IR spectra of chitosan were characterized by the following absorption bands: the (NH) of backbone polymer arising at 3435 and 1630 cm^{-1}, (C–O) of primary alcoholic group at 1382 cm^{-1}, and the (C–H) at 2940 cm^{-1} (Fig. 2a). The interaction between iron oxide core and chitosan can be due to the chelation of electron pairs of oxygen atoms with Fe vacant orbitals as electrostatic interactions. In Fe_3O_4@CS NPs, absorptions of chitosan appear along with a peak at 569 cm^{-1} which corresponds to the stretching vibration of Fe–O groups; indicating that the magnetic Fe_3O_4 NPs is coated by chitosan. This interaction between the negatively charged Fe_3O_4 NPs surface and the positively protonated chitosan donates the IR spectra change. The band appearing at 1375 cm^{-1} is related to the C–O of alcoholic groups of chitosan in the (Fig. 2b). The FT-IR

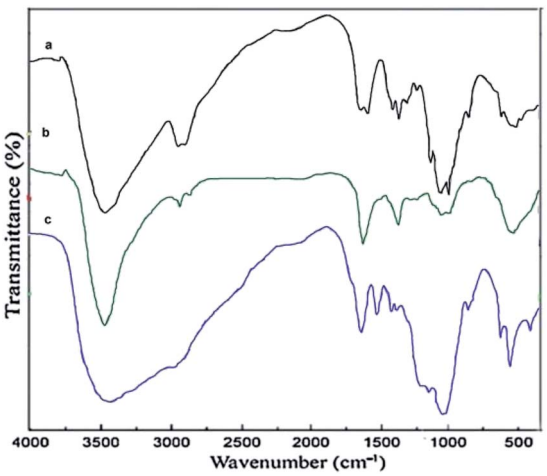

Fig. 2 IR spectrum of (a) chitosan (CS), (b) Fe_3O_4@CS NPs, (c) Fe_3O_4@CS–SO_3HNPs.

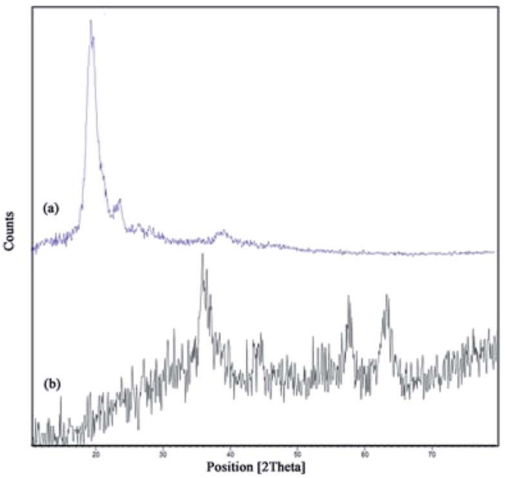

Fig. 3 XRD pattern of (a) chitosan, (b) Fe_3O_4@CS–SO_3H NPs.

spectrum of Fe_3O_4@CS–SO_3H NPs shows the stretching and out-of-plane bending of acidic O–H groups as two broad bands at 2800–3500 and 884 cm^{-1}, respectively. Finally, S–O stretching bands of –SO_3H in O–SO_3H and NH–SO_3H groups were appeared at 1153 cm^{-1} and 1057 cm^{-1}, respectively (Fig. 2c).

3.1.2 X-ray diffraction (XRD) analysis. The crystal structures of chitosan and Fe_3O_4@CS–SO_3H NPs are shown in (Fig. 3). The sharp peaks in the XRD patterns confirm the good crystallinity of the prepared samples. There are six diffraction peaks at 2θ about 31.21°, 36.73°, 43.41°, 53.73°, 57.33° and 63.85° corresponding to (230), (321), (400), (422), (511), and (450) in the Fe_3O_4@CS–SO_3H NPs, which is the standard pattern for crystalline magnetite with cubic structure (JCPDS card no. 01-1111). The small and weak broad bands in the range of 25–28° show the existence of amorphous sulfonated chitosan.

3.1.3 Magnetic properties. The magnetic properties of the as-synthesized Fe_3O_4@CS–SO_3H NPs are measured at room temperature. The negligible coactivity in the magnetization curves indicated that Fe_3O_4@CS–SO_3H NPs are super paramagnetic. A typical magnetization loop appears with the saturation magnetization (M_s) at about 75 emu g^{-1} (Fig. 4). Therefore, catalyst shows high permeability in magnetization which facilitates magnetic separation with a conventional magnet.

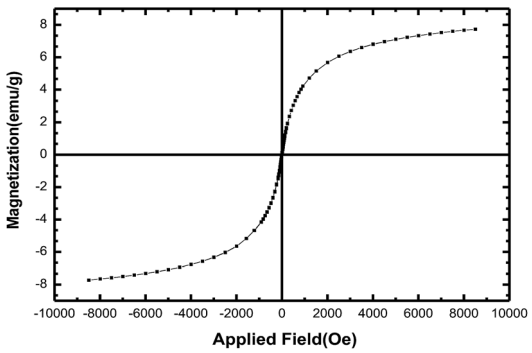

Fig. 4 Magnetization *versus* applied for Fe_3O_4@CS–SO_3H NPs.

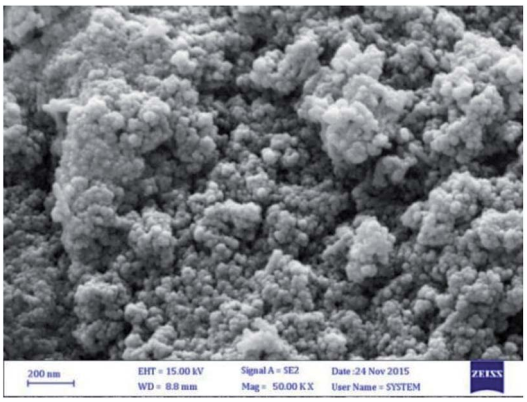

Fig. 5 SEM image of Fe_3O_4@CS–SO_3H NPs.

3.1.4 Scanning electron microscopy (SEM). Fig. 5 exhibits the morphology and particle size of Fe_3O_4@CS–SO_3H NPs. It indicates that the chitosan polymeric matrix is uniformly covered on the surface of Fe_3O_4 NPs (Fig. 5). The SEM image shows that the structure of Fe_3O_4@CS–SO_3H NPs size is bigger. The SEM of Fe_3O_4@CS–SO_3H NPs clearly revealed the structure of the CS-coated magnetite nanoparticle.

3.1.5 Energy dispersive X-ray (EDX). The elemental compositions are calculated from the energy dispersive X-ray (EDX). The elemental compositions of Fe_3O_4@CS–SO_3H NPs are 0.52%, 2.94%, 9.0%, 17.94%, and 69.6% for N, C, S, O and Fe, respectively. This implied that chitosan polymer was coated on the surface of the Fe_3O_4 NPs (Fig. 6).

Furthermore, the total surface acidity for the Fe_3O_4@CS–SO_3H NPs was determined by sodium hydroxide titration. In this measurement procedure, the pH of Fe_3O_4@CS–SO_3H NPs catalyst was 1.02 that can be equal to loading the 2.14 mmol (H^+) g^{-1}.

3.2. Procedures for the synthesis of spiroacridines

After the characterization of the catalyst, in order to optimize the reaction parameters, we investigated the reaction of dimedone (2 mmol), aniline (1 mmol), acenaphthoquinone (1 mmol) in the presence of Fe_3O_4@CS–SO_3H NPs. The model reaction was checked in the presence of different amount of Fe_3O_4@CS–SO_3H NPs as a catalyst at a range of various temperatures and

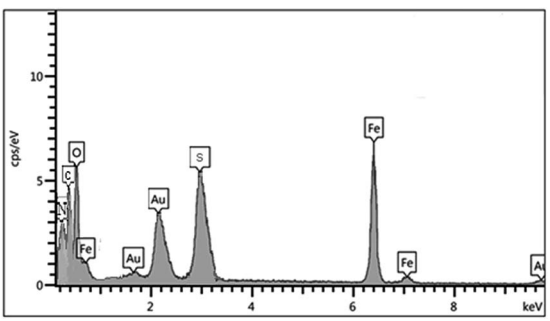

Fig. 6 The energy dispersive X-ray (EDX) of Fe_3O_4@CS–SO_3H NPs.

Table 1 Optimizing the synthesized spiroacridines in the presence of different conditions

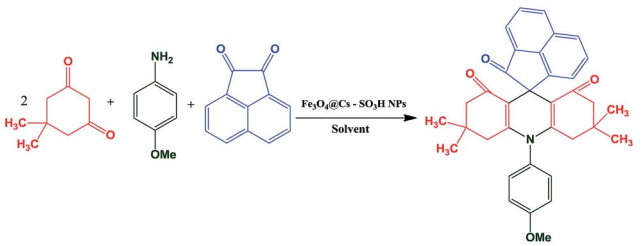

			Heating condition[a]	Ultrasonic irradiation
Entry	Cat. (mg)	Solvent	Time (h)/ Yield[b], %	Time (min)/ Yield[b], %
1	0.3	EtOH/H_2O	2/59	10/78
2	0.5	EtOH/H_2O	2/63	10/78
3	1	EtOH/H_2O	1/68	5/93
4	1.5	EtOH/H_2O	1/68	5/93
5	1	CH_3CN	2/48	20/57
6	1	H_2O	2/—	20/—
7	—	EtOH/H_2O	4/trace	35/42

[a] Under reflux at boiling points of different solvents. [b] Isolated yields.

also under ultrasonic irradiation in various solvents. The results are shown in Table 1. As this table indicates, when the reaction was carried out under harsh heating conditions, it gave low yields of products and took longer reaction times, while the same reaction was carried out under ultrasonic irradiation at room temperature to provide excellent yields of products in short reaction times. Thus, the best results were obtained when the reaction was performed using 1 mg of the catalyst in EtOH/H_2O under ultrasonic irradiation (Table 1, entry 3).

In continuation of this method, the role of ultrasonic irradiation and the effect of various powers of ultrasonic irradiation on the reaction and the reaction under without ultrasound were examined (Table 2). As can be seen in this table, the reaction on the without ultrasound (silent) at room temperature was resulted any product even continued at

Table 2 The effect of ultrasonic irradiation on the formation of spiroacridines[a]

Entry	Power (W)	Time (min)	Yield[b] (%)
1	Silent[c]	150	—
2	25	30	57
3	30	20	74
4	35	15	85
5	40	5	93
6	45	5	93

[a] Dimedone (2 mmol), aniline (1 mmol), acenaphthoquinone (1 mmol) and Fe_3O_4@CS–SO_3H NPs (1 mg). [b] Isolated yields. [c] The reaction at room temperature.

Table 3 Synthesis of various spiroacridines using Fe_3O_4@CS–SO_3H NPs under ultrasonic irradiation (40 W)[a]

Entry	Product	R (amine)	Time (min)	Yield[b] (%)
1	**4a**	4-NO_2–C_6H_4	8	85
2	**4b**	4-OH–C_6H_4	5	93
3	**4c**	4-Cl–C_6H_4	6	87
4	**4d**	4-Br–C_6H_4	6	89
5	**4e**	4-Me–C_6H_4	5	91
6	**4f**	4-OMe–C_6H_4	5	93
7	**4g**	2-OH–C_6H_4	5	90
8	**4h**	2-NO_2–C_6H_4	8	83
9	**4i**	2-Cl–C_6H_4	6	80
10	**4j**	3-NO_2–C_6H_4	9	76
11	**4k**	2,4-Me_2–C_6H_3	5	92
12	**4l**	Phenyl	7	88
13	**4m**	4-H_2N–C_6H_4	8	90
14	**4n**	Thiazolyl	80	N.R.

[a] Dimedone (2 mmol), aniline (1 mmol), acenaphthoquinone (1 mmol) and Fe_3O_4@CS–SO_3H NPs (1 mg). [b] Isolated yields.

150 min. While, replacement of the same reaction under ultrasonic condition at various power were obtained the target product in good to excellent yields (Table 2, entry 1 *vs.* entries 2–6). These results show that the sonication certainly affected the reaction system. The probable explanation for the positive connotation of irradiation is that the ultrasonic irradiation could increase the number of active cavitation bubbles of which are expected to result in higher maximum collapse temperature and speeded respective reaction. We employed various conditions and it was found that the reaction gave satisfying result in the presence of 1 mg of Fe_3O_4@CS–SO_3H NPs under ultrasonic irradiation with the power of 40 W in aqueous ethanol.

We examined condensation reaction under ultrasonic irradiation without catalyst. When the reaction was examined without catalyst, the products were obtained in a moderate to good yields (Table 1). The results show that the sonication certainly affected the reaction system.

We also applied Fe_3O_4@CS–SO_3H NPs in synthesis spiroacridines derivatives from various aromatic amines under similar condition as represented in Table 3. In general, the reactions are clean and high-yielding. Several groups, such as Cl, Br, NO_2, OCH_3, OH and CH_3, are compatible under the reaction conditions. Interestingly, a variety of aromatic amines, including *ortho*, *meta* and *para*-substituted aryl amines, participated well in this reaction and gave the corresponding products in a good to excellent yield (Table 3). The influence of electron-withdrawing and electron-donating substituents on the aromatic ring of amines upon the reaction yields was investigated. These results show that aromatic amines with electron-releasing groups reacted faster than those with electron-withdrawing groups.

The proposed reaction mechanism for synthesis of spiroacridines catalyzed by Fe_3O_4@CS–SO_3H NPs is depicted in Scheme 3. Initially, the Fe_3O_4@CS–SO_3H NPs catalyst protonates the carbonyl group of acenaphthoquinone (**1**), which then

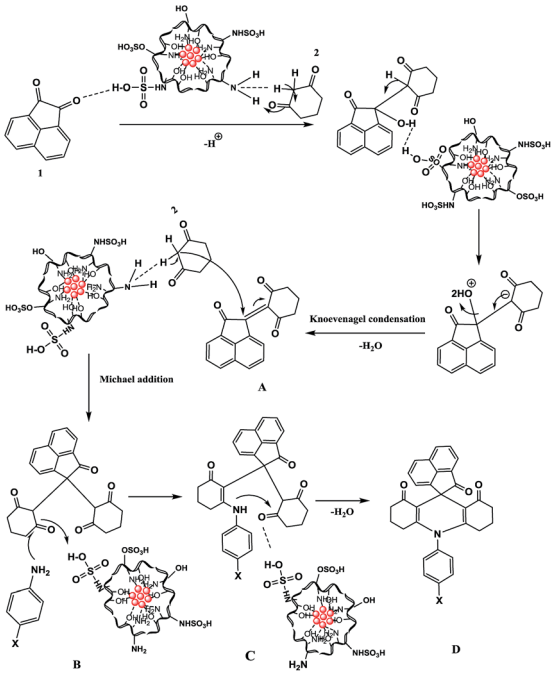

Scheme 3 Plausible mechanism for the synthesis of spiroacridine.

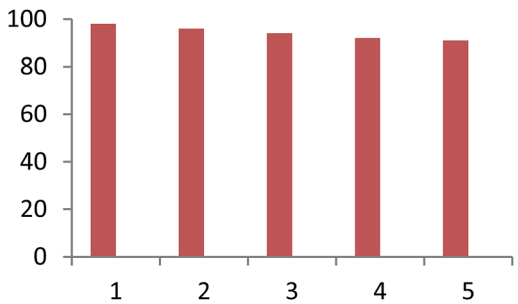

Fig. 7 Reusability of catalyst for synthesis of spiroacridine.

condenses with CH acidic group of dimedone (**2**) through a fast Knoevenagel condensation to afford **A** derivative. Then, dimedone (**2**) participates in a Michael addition with compound **A** to form intermediate **B**, the –NH group of amine which subsequently undergoes an intramolecular attack of the carbonyl group, resulting in a cyclization reaction that affords **C**. Finally, intermediate **C** loses a molecule of H_2O to lead to the formation of acridine **D**.

For practical applications of such heterogeneous system, the reusability is one of the important properties of the catalyst. The reusability of used catalyst was investigated using the reaction of dimedone, aniline and acenaphthoquinone in the presence of Fe_3O_4@CS–SO_3H NPs as a catalyst under sonication condition. The catalyst was isolated by simple filtration, washed exhaustively with water–acetone and dried. The results in five consecutive runs (98%, 98%, 97%, 96% and 96%) indicated the yields remained similar with no detectable loss of yield and catalytic activity under sonication condition (Fig. 7).

4. Conclusions

In this paper, we have described the synthesis of spiroacridine derivatives using dimedone and acenaphthoquinone with substituted aromatic amines, under the action of ultrasonic irradiation, in the presence of Fe_3O_4@CS–SO_3H NPs catalyst. The desired products were obtained in high to excellent yields and high purities with short reaction times. The prepared magnetic catalyst could be easily recovered by simple filtration and the efficiency of the catalyst remains unaltered after several times. Also, we have presented that compared to heating method; ultrasound irradiation can speed up the reaction and is more suitable and efficient.

Acknowledgements

The authors are grateful to the University of Kashan for supporting this work by Grant no. 159148/66.

References

1 J. T. Li, Y. Yin and M. X. Sun, *Ultrason. Sonochem.*, 2010, **17**, 363–366.
2 Y. Zou, Y. Hu, H. Liu and D. Shi, *ACS Comb. Sci.*, 2011, **14**, 38–43.
3 M. Mamaghani and S. Dastmard, *Ultrason. Sonochem.*, 2009, **16**, 445–447.
4 S. J. Ji, Z. L. Shen, D. G. Gu and X. Y. Huang, *Ultrason. Sonochem.*, 2005, **12**, 161–163.
5 A. R. Khosropour, *Ultrason. Sonochem.*, 2008, **15**, 659–664.
6 K. Takahashi, B. Witkop, A. Brossi, M. A. Maleque and E. X. Albuquerque, *Helv. Chim. Acta*, 1982, **65**, 252–261.
7 A. Longeon and M. Guyot, *Experientia*, 1990, **46**, 548–550.
8 J. Kobayashi, M. Tsuda, K. Agemi, H. Shigemori, M. Ishibashi and T. Sasaki, *Tetrahedron*, 1991, **47**, 6617–6622.
9 P. Maloo, T. Kanchan Roy, D. M. Sawant, R. T. Pardasani and M. M. Salunkhe, *RSC Adv.*, 2016, **6**, 41897–41906.
10 D. M. James, H. B. Kunze and D. J. Faulkner, *J. Nat. Prod.*, 1991, **54**, 1137–1140.
11 T. Okita and M. Isobe, *Tetrahedron*, 1994, **50**, 11143–11152.
12 P. Rosemmond, M. M. Hossemi and C. Bub, *Liebigs Ann. Chem.*, 1994, **2**, 151–158.
13 M. J. Kornet and A. P. Tnio, *J. Med. Chem.*, 1976, **19**, 892–898.
14 N. Lashgari and G. Mohammadi Ziarani, *ARKIVOC*, 2012, **41**, 277–320.
15 K. Jadidi, R. Ghahremanzadeh and A. Bazgir, *Tetrahedron*, 2009, **65**, 2005–2009.
16 R. Ranjith Kumar, S. Perumal, P. Senthilkumar, P. Yogeeswari and D. Sriram, *Eur. J. Med. Chem.*, 2009, **44**, 3821–3829.
17 N. Kostevsek, E. Locatelli, C. Garrovo, F. Arena, I. Monaco, I. Petrov Nikolov, S. Sturm, K. Z Rozman, V. Lorusso, P. Giustetto, P. Bardini, S. Biffi and M. C. Franchini, *Chem. Commun.*, 2016, **52**, 378–381.
18 L. Obeid, D. Talbot, S. B. Jaafar, V. Dupuis, S. Abramson, V. Cabuil and M. Welschbillig, *J. Colloid Interface Sci.*, 2013, **410**, 52–58.

19 L. M. Murillo, J. S. Margarida, M. T. F. Telling, J. P. R. L. L. Parra, S. Landsgesell, R. I. Smith and H. N. Bordallo, *J. Alloys Compd.*, 2014, **584**, 514–519.
20 A. Singh and S. K. Sahoo, *Drug Discovery Today*, 2014, **19**, 474–481.
21 X. N. Zhao, H. C. Hu, F. J. Zhang and Z. H. Zhang, *Appl. Catal., A*, 2014, **482**, 258–265.
22 G. Li, Y. Jiang, K. Huang, P. Ding and J. Chen, *J. Alloys Compd.*, 2008, **466**, 451–456.
23 X. Li, S. Zhang, B. Yang, C. Lv, X. Jia and Z. Hu, *RSC Adv.*, 2016, **6**, 86531–86539.
24 A. Pourjavadi, A. Motamedi, S. H. Hosseini and M. Nazari, *RSC Adv.*, 2016, **6**, 19128–19135.
25 M. N. Shaikh, M. A. Aziz, A. Helal, M. Bououdina, Z. H. Yamani and T. J. Kim, *RSC Adv.*, 2016, **6**, 41687–41695.
26 J. Qu, G. Liu, Y. Wang and R. Hong, *Adv. Powder Technol.*, 2010, **21**, 461–467.
27 C. Yuwei and W. Jianlong, *Chem. Eng. J.*, 2011, **168**, 286–292.
28 X. Chen, H. Yang and N. Yan, *Chem.–Eur. J.*, 2016, **22**, 13402–13421.
29 N. Yan and X. Chen, *Nature*, 2015, **524**, 155–157.
30 B. Karami, K. Eskandari and A. Ghasemi, *Turk. J. Chem.*, 2012, **36**, 601–614.

